Thermodynamics of attractor enlargement

K. G. Szabó and T. Tél
Institute for Theoretical Physics, Eötvös University Budapest, Puskin utca 5-7, Budapest, H-1088, Hungary
(Received 26 January 1994)

Sudden enlargement of a small-size chaotic attractor occurs when it collides with a coexisting nonattracting chaotic set. Before the collision the two dynamically independent invariant sets are characterized by different thermodynamical potentials, e.g., by free energies. The infinitesimally weak dynamical coupling appearing at crisis generates a third component, and the resultant free energy of the enlarged attractor is obtained as the minimum of the three partial free energies. Not far beyond the crisis the free energy of the enlarged attractor is still very close to the minimum of those belonging to the remnant of the old attractor and the other nonattracting chaotic set. We demonstrate this general phenomenon by one-dimensional maps. By extending the concept of Frobenius-Perron operators we invent the constrained generalized Frobenius-Perron operator providing us with a method to compute the free energies of invariant chaotic sets which are either coexisting side by side each other independently or being embedded in a larger set.

PACS number(s): 05.45.+b

I. INTRODUCTION

Dramatic changes in the structure of chaotic attractors might take place as some control parameter a passes through certain critical values. These changes can be either sudden *destructions* or *enlargements* of attractors or *attractor mergings*. Such critical situations, called crisis situations [1], attracted recent interest from both experimental [2–4] and theoretical [5–14] points of view. Attractor enlargement, which is experimentally most accessible, occurs, for example, at one edge of any periodic window within the chaotic regime of any dynamical system.

From a dynamical point of view, the geometric change of the size and shape of the attractor is accompanied in such cases by the phenomenon of the so-called crisis induced intermittency [7]. This means that trajectories on the attractor somewhat past the critical value a_c stay in the phase space region of the precritical chaotic attractor for some time, then burst into a chaotic motion over a larger region before turning back to the original region again. This process then repeats again and again, however, the duration of the chaotic motions in the region of the former attractor varies unpredictably. Crisis induced intermittency can be characterized by the average time τ between subsequent bursts which tends to infinity as the critical value a_c is approached.

The key observation [15] in understanding the phenomenon of attractor enlargement is that the precritical chaotic attractor, which may well consist of several disjoint pieces, coexists with a *nonattracting chaotic set* (either a saddle or a repellor [16]). The attracting and nonattracting sets are independent in the sense that they have two different natural invariant measures not connected dynamically. While gradually approaching the crisis point, the nonattracting set changes only hardly and smoothly, but the attractor becomes closer and closer to its fully developed chaotic state. The crisis configuration is that special situation when the attractor just touches its basin boundary on which the nonattracting chaotic set sits. By this touch, a heteroclinic connection is created between the unstable manifold of the attractor and the stable manifold of the nonattracting set. Due to this dynamical coupling, beyond crisis there exists only a single enlarged chaotic attractor which contains both of the former attracting and nonattracting invariant sets. In the postcritical region the remnant of the old multipiece attractor also becomes a nonattracting chaotic set (via the same mechanism as for attractor destruction). It coexists with the other — practically unchanged — nonattracting chaotic set. The two sets are connected via heteroclinic tangles. In particular, the average lifetime of trajectories staying in the close neighborhood of the new nonattracting set practically equals the average time between bursts into the region which has not belonged to the precritical attractor [7].

We would like to emphasize that attractor enlargement provides a good example for multitransient chaos [17] where the dynamics of weakly coupled nonattracting chaotic sets can be successfully used to analyze the motion on the joint chaotic attractor.

The thermodynamical formalism [18] of dynamical systems has proved to be a powerful method in characterizing chaotic motion. It is a question of principal interest how it should be applied when two or more chaotic sets coexist, as in the case of attractor enlargement before and after crisis.

In this paper we point out that in the precritical region two different free energies [19] characterize the system: one for the attracting and another one for the nonattracting chaotic set. They are associated with different sorts of dynamics: permanent and transient chaos, and are, therefore, independent. It is to be emphasized that although transient chaos reflects the properties of a set with a basin of attraction of measure zero, the chaotic motion on this set is *more pronounced* than the one on

the attractor in the sense that it has greater Lyapunov exponent and topological entropy.

At crisis the two sets become coupled, although first in an extremely weak manner only. Consequently, the free energy for the union of these sets is just the *absolute minimum* of the two partial free energies. Because of taking the minimum, the resultant free energy will show a break at some inverse temperature. At the very same crisis point a third component appears as well: the *heteroclinic connection.* Since this component is just at birth, it is connected with a marginally stable periodic orbit. Consequently, the free energy of this component is equal to zero and practically independent of the other two components. Thus another break shows up which makes the resultant free energy identically zero for $\beta \geq 1$.

Beyond crisis the remnants of the precritical chaotic sets are no longer independent. It is nevertheless worth dealing with their partial free energies characterizing the corresponding subdynamics. The resultant free energy is now somewhat below the absolute minimum of the partial ones and does not exhibit any nonanalyticity.

In order to be specific, we study one-dimensional maps around the end of periodic windows which are accompanied by crisis induced intermittency. In such one-dimensional cases the use of generalized Frobenius-Perron operators (FPO's) [20–28], whose largest eigenvalue directly yields the free energy, has proved to be very efficient. We show that different partial free energies arise by choosing the functions on which the generalized FPO acts from *different function spaces.* Technically we introduced the concept of *constrained* generalized FPO's that are restricted to certain subsets X of the entire interval on which the map is defined. The constrained FPO is shown to yield the free energy of the invariant set that is contained in region X.

The paper is organized as follows. In Sec. II the invariant chaotic sets relevant for the phenomenon of attractor enlargement are described. Next, we define the corresponding cylinder sets and free energies. The constrained FPO is introduced in Sec. IV. The numerical methods applied and the free energies characterizing the precritical, critical, and postcritical situations are presented in Sec. V. In the last section, in addition to some general remarks, we give a description of attractor enlargement in terms of another thermodynamical potential, the entropy, obtained as the Legendre transform of the free energy.

II. INVARIANT SETS AROUND CRISIS INDUCED INTERMITTENCY

As a working example we chose the main period-3 window of the quadratic map

$$x_{n+1} = f(x_n) = a - x_n^2 \tag{1}$$

lying in the parameter range $1.75 < a < a_c \equiv 1.790\,327\,491\,99\ldots$, which has been studied intensely in the literature [1].

The attractor enlargement takes place at the critical value a_c. We briefly summarize the topological changes in the phase space structures as a passes through this critical value from below.

A. Precritical situation

Figure 1(a) shows that slightly below a_c the map f restricted to three bands $B_1 \equiv (x_A, x_a)$, $B_2 \equiv (x_b, x_B)$, and $B_3 \equiv (x_C, x_c)$ has the following property: B_2 is mapped onto B_3, B_3 onto B_1, and B_1 *into* B_2; the latter follows since the image of the maximum point of the parabola, $f(0) = a$, is less than x_B. Therefore these intervals form a primary range of attraction with three pieces of the chaotic attractor located inside. The boundary points of this range are the unstable period-3 points x_a, x_b, and x_c, together with three subsequent preimages of x_b: x_A, x_C, and x_B (cf. Fig. 1).

It is worth considering the effect of the mapping on the two gaps in between the three parts of the attractor. Gap $G_1 \equiv [x_c, x_A]$ is mapped onto gap $G_2 \equiv [x_a, x_b]$, but G_2 is mapped onto $[x_c, x_b] = G_1 \cup B_1 \cup G_2$. Thus the map restricted to $G_1 \cup G_2$ is *not closed* in dynamical sense: typical trajectories started from here sooner or later leave this region by being mapped into B_1. However, there exist periodic orbits of infinite number in this region (likewise aperiodic ones) which never escape. These orbits form another invariant set besides the attractor and the external fixed point $x_* \equiv -[1/2 + (a + 1/4)^{1/2}]$. Since all orbits on this nonattracting set of measure zero are strictly repelling, it is called the *chaotic repellor.* The repellor is located within the two intervals G_1 and G_2, therefore it will be referred to as the "two-piece repellor" in the following, for simplicity.

Thus in the precritical situation there are two dynamically independent chaotic sets in the system: the three-piece attractor and the two-piece repellor, producing permanent and transient chaotic behavior, respectively. We would like to draw attention to the fact that the period-3 points x_a, x_b, and x_c, the boundary points of the range of attraction, are the sidepoints of the repellor, at the same time.

B. The crisis situation

At $a = a_c$ [see Fig. 1(b)] the maximum point is just mapped on x_B, thus the three-piece chaotic attractor extends to the whole primary range of attraction (B_1, B_2, and B_3). This fully developed chaotic attractor touches the repellor at the boundary points, thus the unstable period-3 orbit now belongs to both the three-piece attractor and the two-piece repellor. The existence of a common periodic orbit will be reflected in the dynamical properties.

C. Postcritical situation

If the control parameter is increased beyond the crisis value a_c, then $a = f(0) > x_B$ and the maximum point

is mapped outside B_2 [see Fig. 1(c)]. Since the image of the interval B_1 sticks out of B_2, the map restricted to the former three-piece range of attraction is not closed any longer. In fact, the chaotic attractor undergoes a sudden enlargement: it becomes a one-piece attractor by extending to the whole interval $A \equiv [f(a), a]$, which includes both the bands of the former three-piece attractor and the gaps where the two-piece repellor was located.

The former chaotic sets, however, did not disappear without a trace. It is possible to distinguish those orbits that never leave the two-piece gap region $G \equiv G_1 \cup G_2$ in which one, therefore, finds a two-piece repellor again. Analogously, it is also possible to define a set consisting

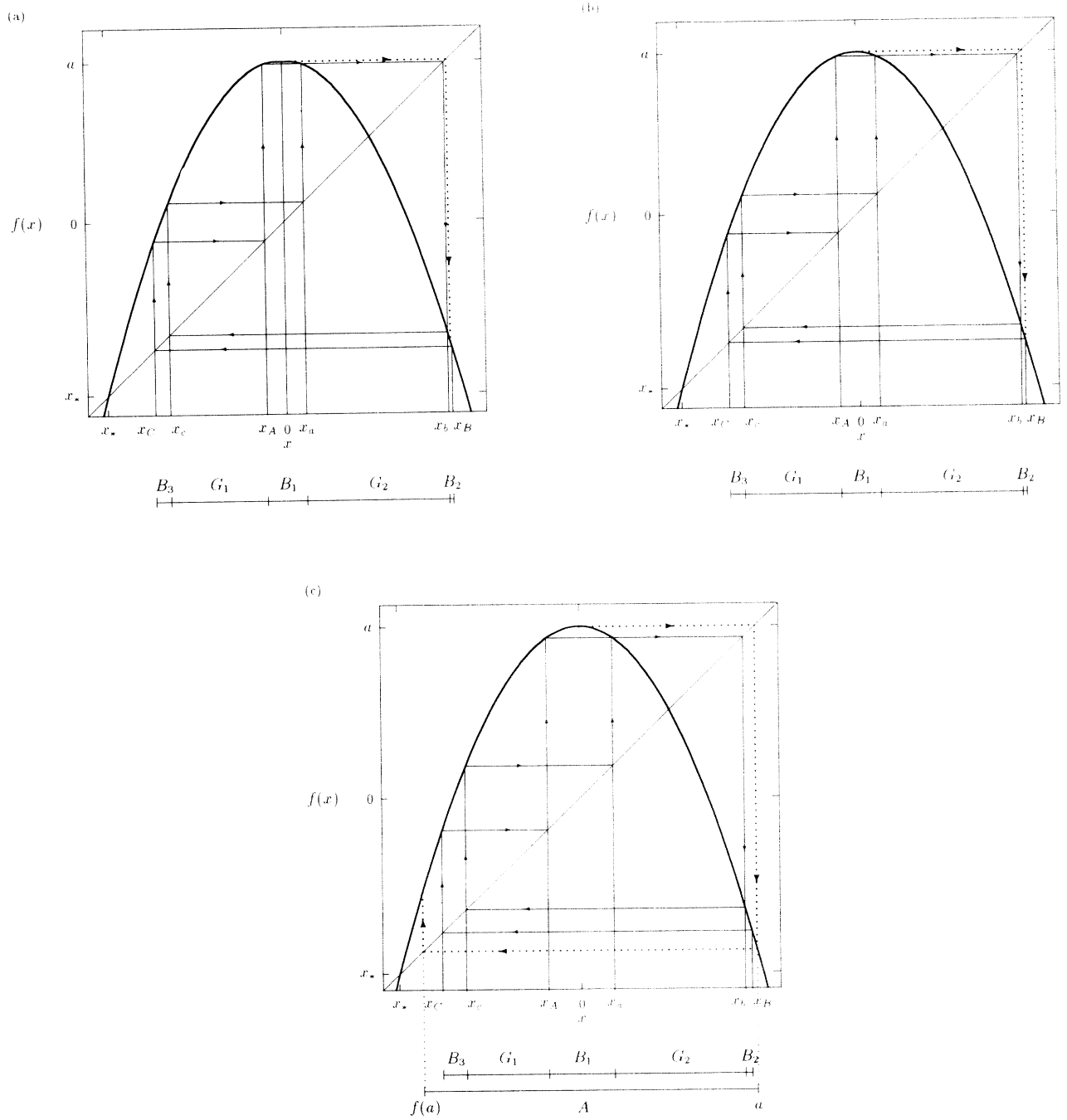

FIG. 1. The quadratic map (1) and the natural coverage of its basic invariant sets around attractor enlargement. x_* denotes the external unstable fixed point. The mediating period-3 orbit (x_a, x_b, x_c) and the points x_A, x_C, and x_B on its stable manifold determine the end points of the band (B) and gap (G) regions. The arrows indicate how these are mapped onto each other. The dotted line shows that in the precritical (a), critical (b), and postcritical (c) cases the maximum point is mapped into B_2, exactly on x_B, and outside of B_2, respectively. In the latter case the first two images of the origin define the edges of the enlarged attractor (A). The actual control parameter values were $a = 1.785$ (a), $a_c = 1.7903\ldots$ (b), and $a = 1.8$ (c).

of orbits that never escape from the band region $B \equiv B_1 \cup B_2 \cup B_3$. This set will be called hereafter the three-piece repellor arising beyond crisis as the remnant of the three-piece attractor.

It may be worth mentioning that the shape of the two-piece repellor practically does not change while the system is passing through the crisis: it has wide gaps and a relatively small fractal dimension. On the other hand, while departing from the crisis point the gaps of the three-piece repellor open up. Their width is proportional to $(a-a_c)^{1/2}$, so the fractal dimension of this set is very close to 1 around a_c. The period-3 orbit $\{x_a, x_b, x_c\}$ on the boundary between the two- and the three-piece repellors belongs to both invariant chaotic subsets.

Although being only zero measure subsets of the whole attractor, these two repellors basically determine the dynamical behavior of the system if a is not very far from the crisis value. In this case the heteroclinic coupling between the two regions is so weak that the dynamics of the system can be considered as intermittent switchings between two sorts of transient chaotic behaviors: long chaotic paths in the three-piece region escape to the two-piece region, from where relatively short chaotic transients, bursts, lead back to the three-piece region again.

III. THERMODYNAMICAL QUANTITIES

A. Cylinders and free energy

The thermodynamical formalism of one-dimensional dynamical systems is based on the definition of a hierarchically nested set of intervals, the so-called cylinders [18,19].

As the first step of cylinder construction the chaotic set has to be covered with a single "level-0" cylinder. This covering has to be refined to a level-1 partition so that the map restricted to each partition interval is continuous and invertible. The level-1 cylinders are then defined by taking within each partition the closest possible coverage of the chaotic set. Each level-1 cylinder can be further divided by taking its intersections with the preimages of every level-1 cylinder set one by one. Then the coverage can be refined again by taking new, level-2 covering cylinders within each intersection. Repeating this process iteratively one obtains the whole hierarchy of cylinder sets.

The partition at the first level is called the generating partition [18] if it is chosen so that in the resulting hierarchy the maximal length of level-n cylinders vanishes as $n \to \infty$. In the cases investigated in this study, this criterion always holds.

Let the set

$$\{\ell_1^{(n)}, \ell_2^{(n)}, \ldots, \ell_{N(n)}^{(n)}\} \tag{2}$$

contain the lengths of level-n cylinders, where $N(n)$ denotes the total number of cylinders.

The number of cylinders increases exponentially,

$$N(n) \sim e^{K_0 n}, \tag{3}$$

for large n's where the exponent K_0 is the topological entropy of the set.

The fractal dimension, D_0, of the chaotic set can also be obtained in the large n limit from the implicit equation

$$\sum_{i=1}^{N(n)} (\ell_i^{(n)})^{D_0} = \text{const.} \tag{4}$$

In the case of repellors D_0 is less than one, and the total length of the covering cylinders vanishes exponentially when $n \to \infty$:

$$\sum_{i=1}^{N(n)} \ell_i^{(n)} \sim e^{-\kappa n}. \tag{5}$$

Here κ denotes the escape rate from the invariant set.

The *free energy function* of the chaotic set based on the cylinder construction is defined [19] by the asymptotic scaling relation

$$\sum_{i=1}^{N(n)} (\ell_i^{(n)})^{\beta} \sim e^{-\beta F(\beta) n}. \tag{6}$$

As a fundamental thermodynamical potential, the free energy function can be used to derive important dynamical scaling quantities. For example, a direct comparison to the definitions (3), (5), and (4) shows that the topological entropy, the escape rate, and the fractal dimension of an invariant set can be extracted from the $\beta F(\beta)$ function by taking it at $\beta = 0$ [$K_0 = -\lim_{\beta \to 0} \beta F(\beta)$], at $\beta = 1$ [$\kappa = F(1)$], and by determining its root [$F(D_0) = 0$], respectively. It can be shown [19] that the average Lyapunov exponent λ (taken with respect to the natural measure) is the derivative of $\beta F(\beta)$ at $\beta = 1$: $\lambda = [\beta F(\beta)]'_{\beta=1}$.

B. Construction of cylinders around crisis

Now we carry out the construction of cylinders for each chaotic invariant set. First we show the cylinder construction of the attracting chaotic sets, then the construction for the nonattracting ones.

a. The one-piece postcritical attractor beyond crisis is the interval $A = (f(a), a)$ [cf. Fig. 1(c)]; we consider it as the level-0 cylinder set. By cutting this interval at $x = 0$, one obtains two subintervals, $C_0^{[A]} \equiv (f(a), 0)$ and $C_1^{[A]} \equiv (0, a)$, on which the map is monotonous [Fig. 2(a)]. We take $C_0^{[A]}$ and $C_1^{[A]}$ as the level-1 cylinders. These latter intervals, being the preimages of the attractor, occupy more space than the attractor itself. Therefore the level-2 cylinders then can be obtained by taking the intersections $C_{ij}^{[A]} \equiv C_i^{[A]} \cap f^{-1}[C_j^{[A]}]$ $(i,j = 0,1)$, allowing that some of these may be empty. Similarly, the level-3 cylinders can be obtained from the level-2 cylinders by splitting them according to their preimages: $C_{ijk}^{[A]} \equiv C_{ij}^{[A]} \cap f^{-1}[C_{jk}^{[A]}] = C_i^{[A]} \cap f^{-1}[C_{jk}^{[A]}]$ $(i,j = 0,1)$, etc. The number of symbol subscripts gives n, the level in the hierarchy.

The number of cylinders is at most doubled in each step

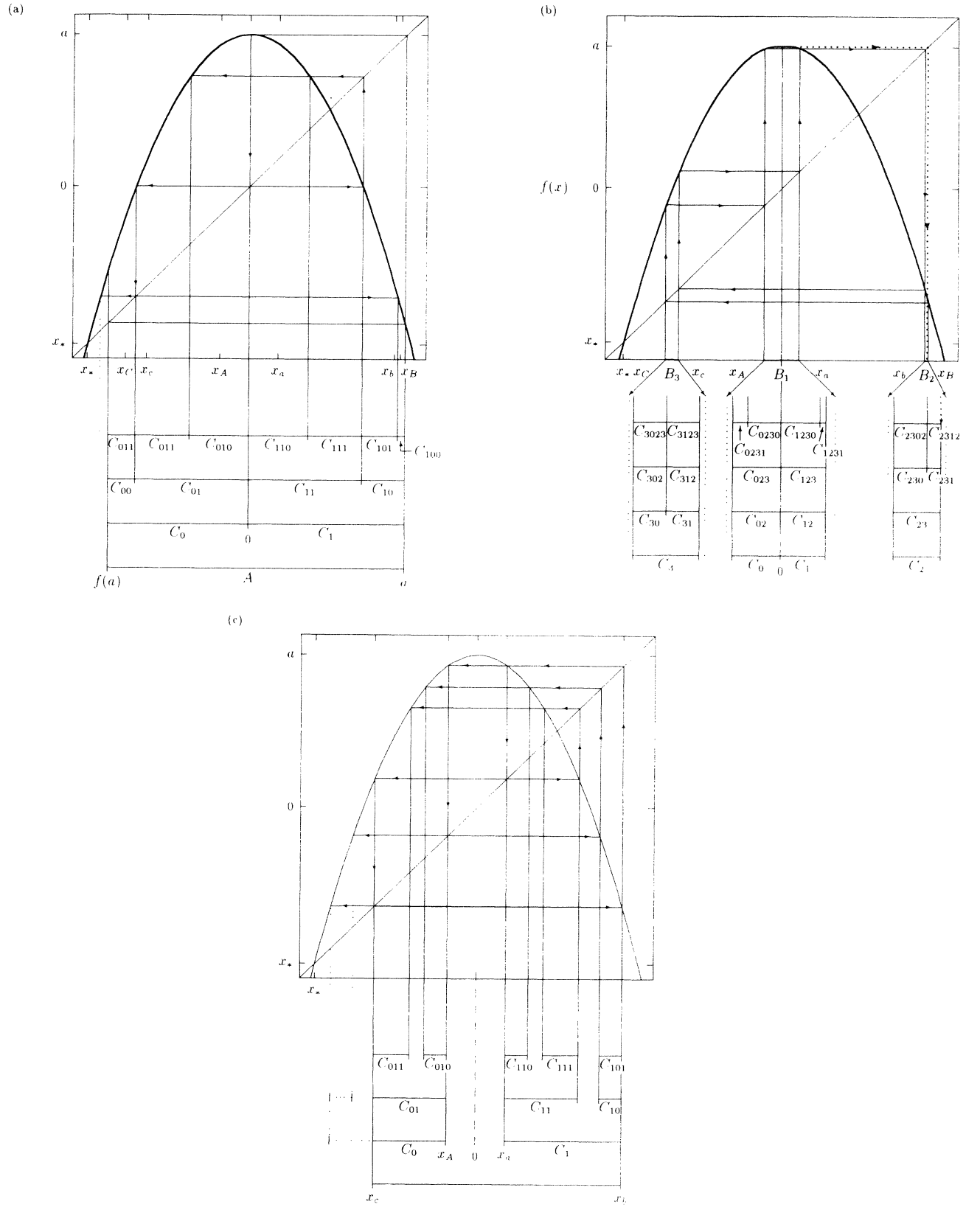

FIG. 2. The construction of the generating partition and the first few level of cylinders of the enlarged attractor (A) at $a = 1.8$ (a), the precritical attractor ($A3$) (b), and the precritical repellor in G (c) at $a = 1.785$. The attractor constructions give joint cylinders with incomplete symbolic grammars since $a \neq a_c$. The repellor construction, yielding disjoint cylinders whose number follows the Fibonacci sequence, goes exactly the same way in the postcritical regime as shown here.

of the construction: $N^{[A]}(n) \leq 2^n$. According to (3), this yields the obvious upper limit

$$K_0^{[A]} \leq \log(2) \tag{7}$$

for the topological entropy of the enlarged attractor.

The ensemble of the lengths of cylinders $C^{[A]}_{i_1 i_2 \ldots i_n}$ provides the length set

$$\{\ell_i^{[A](n)}\}_{i=1,\ldots,N^{[A]}(n)}$$

associated with attractor A.

b. The three-piece precritical attractor ($A3$), located within the band region B [cf. Fig. 1(a)], provides a good example to show how the cylinder construction of the attractor differs when it consists of several pieces.

In this case a partition of four level-1 cylinders is required to cover the attractor [see Fig. 2(b)]: $C_2^{[A3]} \equiv [f^{(4)}(0), f(0)]$ covers the right piece of the attractor within B_2; $C_3^{[A3]} \equiv [f^{(2)}(0), f^{(5)}(0)]$ the left piece within B_3; while $C_0^{[A3]} \equiv [f^{(3)}(0), 0]$ and $C_1^{[A3]} \equiv [0, f^{(6)}(0)]$ cover the monotonous parts within B_1. The cylinders at subsequent levels then can be constructed along the same lines as it was done in the case of the one-piece attractor [cf. Fig. 2(a)].

An alternative method of construction is based upon the constrained visiting order $B_1 \to B_2 \to B_3 \to B_1 \cdots$ of the three pieces. Therefore it is possible to construct the cylinders of the attractor of the third iterated map $f^{(3)}$ within the central band B_1, using the first order partition to $C_0^{[A3]}$ and $C_1^{[A3]}$, as defined above. The level-$3n$ cylinders of the three-piece attractor can then be obtained by taking the level-n cylinders of the threefold iterated attractor and their first and second preimages within B_3 and B_2. This method of construction implies the upper limit

$$K_0^{[A3]} \leq \frac{1}{3}\log(2) \tag{8}$$

for the topological entropy.

In the crisis situation, at $a = a_c$, the three pieces of the attractor exactly fill up the three bands B_1, B_2, and B_3. The inequality in the previous expression for the topological entropy is then replaced by an equality.

c. The two-piece repellor [see Fig. 2(c)]. The level-0 coverage of this set is the interval $[x_c, x_b] = G_1 \cup B_1 \cup G_2$. This is to be divided in the next step at $x = 0$ into two pieces on which the map is invertible. Excluding B_1, which does not contain points of the two-piece repellor, leads us to choose $C_0^{[G]} = G_1$ and $C_1^{[G]} = G_2$ as level-1 partition sets. Note that B_1 is the only way out from this region, thus by excluding its order-n preimages, one can obtain the points not escaping in n steps. Consequently, the level-n cylinder sets $C^{[G]}_{i_1 i_2 \ldots i_n} \equiv C^{[G]}_{i_1} \cap f^{-1}[C^{[G]}_{i_2 i_3 \ldots i_n}] = f_{i_1}^{-1}[C^{[G]}_{i_2 i_3 \ldots i_n}]$ (where f_0^{-1} and f_1^{-1} stand for the inverse of f for the left- and right-hand branch, respectively), are just the complements of the order-n preimages of B_1. In the $n \to \infty$ limit this construction ends up with the Cantor set structure of the repellor, for which

$$\sum_{i=1}^{N^{[G]}(n)} \ell_i^{[G](n)} \to 0. \tag{9}$$

Using Eqs. (4) and (5) yields a nontrivial fractal dimension $D_0^{[G]} < 1$ and a positive escape rate $\kappa^{[G]}$ for the two-piece repellor.

It is simple to show that the number of cylinders follows the Fibonacci sequence, which results in

$$K_0^{[G]} = \log\left(\frac{\sqrt{5}+1}{2}\right). \tag{10}$$

The above consideration for the construction of the two-piece repellor is independent of whether the system is beyond or above crisis. Therefore the topological entropy of the repellor *does not change* when the attractor undergoes crisis.

d. The three-piece postcritical repellor ($R3$) replacing the precritical attractor beyond crisis can be constructed in the simplest way by again taking advantage of the restricted visiting order of the bands B_i. Then one can construct the level-n cylinders of the repellor of the third iterated map within band B_1 by excluding the higher and higher order preimages of the small "principal band" around 0. The cylinders of the three-piece repellor at level $3n$ can be obtained by taking two subsequent preimages (with respect to the map f) of this structure. The resulting repellor will then be three copies of a diadic Cantor set, one in each band B_i, with a nontrivial fractal dimension $D_0^{[R3]} < 1$ and a topological entropy

$$K_0^{[R3]} = \frac{1}{3}\log(2). \tag{11}$$

C. The free energies of invariant sets

According to Eq. (6), the free energies of the chaotic sets can be extracted from the asymptotic scaling relations

$$\sum_{i=1}^{N^{[X]}(n)} (\ell_i^{[X](n)})^\beta \sim \exp[-\beta F^{[X]}(\beta) n], \tag{12}$$

where the superscripts $X{=}A, G, A3$, and $R3$ in the square brackets distinguish quantities belonging to the postcritical enlarged attractor, the two-piece repellor, the precritical three-piece attractor, and the postcritical three-piece repellor, respectively.

Because the construction of the three-piece attractor and repellor are done the same way, there is a trivial transition between the resulting cylinder structures with lengths $\{\ell_i^{[A3](n)}\}$ and $\{\ell_i^{[R3](n)}\}$, respectively. Therefore it is possible to introduce a single free energy function

$$F^{[B]}(\beta) \equiv \begin{cases} F^{[A3]}(\beta) & \text{if } a \leq a_c \\ F^{[R3]}(\beta) & \text{if } a > a_c \end{cases} \tag{13}$$

for the "three-piece" invariant set located in the band region B.

Knowing the functions $F^{[X]}$, it is possible to determine all dynamical quantities such as $K_0^{[X]}$, $D_0^{[X]}$, $\lambda^{[X]}$, or $\kappa^{[X]}$ corresponding to the respective chaotic sets.

IV. THE CONSTRAINED FROBENIUS-PERRON OPERATOR METHOD

The determination of the cylinders (2) and their length scaling relation (6) is a reliable way for the numerical approach of the free energy function. However, the use of the generalized Frobenius-Perron operator, $\hat{H}_\beta$, defined [20] via

$$\hat{H}_\beta \psi(x') = \sum_{\{x|f(x)=x'\}} \frac{\psi(x)}{|f'(x)|^\beta} \tag{14}$$

provides an even more powerful method. It has already been successfully used to determine the spectrum of dynamical scaling exponents both for chaotic attractors and repellors in cases when there is only one chaotic set in the map. Starting from an arbitrary initial function ψ_0, the consecutive use of the operator yields a sequence of functions:

$$\psi_n(y) = \hat{H}_\beta^n \psi_0(y) = \sum_{\{x|f^{(n)}(x)=y\}} \frac{\psi_0(x)}{|f^{(n)\prime}(x)|^\beta}. \tag{15}$$

The asymptotic growth rate of these functions, $\lambda_1(\beta) \equiv \lim_{n\to\infty} |\psi_n(y)/\psi_0(y)|^{1/n}$, is unique for almost all smooth initial functions and independent of y. It can be interpreted as the largest eigenvalue of $\hat{H}_\beta$ which has been shown [20,27] to be related to the above-defined free energy through

$$\lambda_1(\beta) = e^{-\beta F(\beta)}. \tag{16}$$

In this section we discuss how the generalized FPO can be applied to dynamical maps with coexisting chaotic invariant sets. Let us suppose first that a region G contains a chaotic repellor within the range of attraction of a disjoint chaotic attractor B. We consider two examples below to demonstrate that in such cases the growth rate $\lim_{n\to\infty} |\psi_n(y)/\psi_0(y)|^{1/n}$ depends on y, as well as on the particular choice of the initial function ψ_0.

As the first example we study the case $\beta = 1$ (the conventional FPO). In this case the operator describes the time development of probability distributions due to the map f. Thus any normalized smooth initial function can be considered as a probability density function which asymptotically "shrinks" to the attractor and approaches the density function of the natural measure. Because the natural measure is invariant, the eigenvalue $\lambda_1(1) \approx \psi_n(y)/\psi_{n-1}(y)$ will be 1 for all y points on the attractor. This, by (16), yields $\beta F(\beta) = 0$. (The corresponding eigenfunction of $\hat{H}_1$ is the natural density itself.) However, if y is chosen on the repellor, one finds that the density asymptotically decays with the escape rate κ of the repellor: $\psi_n(y)/\psi_{n-1}(y) \approx e^{-\kappa n}$, yielding a different free energy value, $\beta F(\beta) = \kappa$.

Let us now take the $\beta = 0$ case. If the initial function $\psi_0(x) \equiv 1$ everywhere then, according to (15), $\psi_n(y)$ simply gives the number of the order-n preimages of a point y:

$$\psi_n(y) = \sum_{\{x|f^{(n)}(x)=y\}} \frac{\psi_0(x)}{1} = \sum_{\{x|f^{(n)}(x)=y\}} 1. \tag{17}$$

We would like to remark that there is a significant asymmetry between the dynamical roles of the two chaotic invariant sets: any point y of the attractor has preimages both on the attractor and on the repellor, while points on the repellor have preimages only on the repellor itself. Thus, if y belongs to the repellor, the growth rate of expression (17) is governed by the topological entropy of the repellor. If, however, y belongs to the attractor, the number of its preimages on the attractor and of those on the repellor increase with different topological entropies. The resulting growth rate thus will be dominated by the maximum of the two exponents. In contrast to the $\beta = 1$ case, the ψ_n functions do not shrink asymptotically to the attractor.

By taking different initial functions at $\beta = 0$, the local growth rates may change as well. If $\psi_0(x)$ is chosen to be 1 on the attractor B and 0 elsewhere, then Eq. (15) reads

$$\psi_n(y) = \sum_{\{x|f^{(n)}(x)=y\}} \frac{\psi_0(x)}{1} = \sum_{\{x\in B|f^{(n)}(x)=y\}} 1, \tag{18}$$

i.e., $\psi_n(y)$ counts those order-n preimages of y that lie on the attractor. Therefore if y is on the attractor, $\psi_n(y)$ grows exponentially according to the topological entropy of the attractor, while if y lies outside the attractor, $\psi_n(y)$ remains 0 for any n since it has no preimages in B [cf. Eq. 18]. Along similar lines, it is easy to see that choosing $\psi_0(x)$ so that it is 1 on the repellor and 0 elsewhere yields the same growth exponent, the topological entropy of the repellor on both sets.

These examples show that in the case of coexisting disjoint invariant sets the generalized FPO method as outlined above does not provide us with a unique free energy function. But, as (18) shows, by a careful selection of y points and initial functions, it is possible to avoid the contribution of the unwanted invariant set(s). This has led us to extend the concept of the FPO by involving the necessary constraints into the operator itself. Therefore we define the generalized Frobenius-Perron operator *constrained* to a closed set X (constrained FPO) as

$$\hat{H}_\beta^{[X]} \psi(x') = \begin{cases} \displaystyle\sum_{\{x\in X|f(x)=x'\}} \frac{\psi(x)}{|f'(x)|^\beta} & \text{if } x' \in X \\ 0 & \text{otherwise.} \end{cases} \tag{19}$$

(We do not require X to be contiguous: it may consist of several intervals as well.) This operator acts on a space of functions with their support restricted to X.

Note that using the operator iteratively n times, the sum

$$\psi_n(y) = \hat{H}_\beta^{[X]n}\psi_0(y) = \sum_{\substack{\{x|f^{(n)}(x)=y \\ \forall m=0,1,\ldots,n: f^{(m)}(x)\in X\}}} \frac{\psi_0(x)}{|f^{(n)\prime}(x)|^\beta} \tag{20}$$

takes into account only orbits that remain within X during all the n steps. If there is an invariant (nonwandering) subset inside X, i.e., orbits never escaping this region, then the points x in the sum above converge to this subset. This subset is typically a fractal repellor. As $n \to \infty$ (20) reflects the properties of the invariant subset *within* X only.

The essential difference between formulas (15) and (20) is that the former takes into consideration the reflux of trajectories to X, provided the dynamics allows this, while (20) describes just the contribution from the invariant set inside X without any feedback to other parts of the phase space. By using the constrained operator with a suitably chosen X one can get rid of the initial function or y dependence of the iteration.

When there are several disjoint invariant sets, X should be set so as to contain only the one in question. Then the growth rate of the ψ_n functions yields the first eigenvalue, $\lambda_1^{[X]}(\beta)$, of the operator $\hat{H}_\beta^{[X]}$ for (almost) all y points within X and initial functions restricted to X. The free energy $F^{[X]}(\beta)$ describing the dynamics of the investigated invariant set then follows from (15).

For example, choosing $X=G$ or $X=B$ in the quadratic map (1) makes it possible to determine the free energy functions $F^{[G]}(\beta)$ or $F^{[B]}(\beta)$ of the two-piece repellor or the three-piece attractor, respectively, in the precritical parameter range.

The possible use of the constrained FPO is, of course, not restricted to disjoint invariant sets. The "filter" set X can be chosen arbitrarily, and the corresponding free energy function will give the dynamical scaling exponents of the invariant subset within X only. For example, one can use the cylinder construction scheme as described in Sec. III A and specify X as the union of certain cylinders so as to exclude or include paths with selected symbolic sequences. The FPO constrained to this X then can be used to analyze this artifically pruned dynamics.

This method can be applied in the postcritical regime ($a > a_c$) of the quadratic map (1). The natural choices are the two-piece and three-piece repellors, embedded in the attractor as described in Sec. III, whose free energy functions can be obtained by setting $X=G$ or $X=B$, respectively. Of course, by choosing $X=A$, one can obtain the free energy of the enlarged attractor as well.

V. RESULTS

A. Numerical methods

We compared the cylinder construction method (cf. Sec. III) and the FPO method (Sec. IV). Our experience has shown that the latter method can be used more successfully.

When using the FPO technique, one applies the same operator (and, therefore, the same computer program) for the determination of the free energy functions of all different invariant sets. The only thing one has to do is to adjust X, the support domain of the function space, properly by specifying it as the union of the level-1 cylinders. On the other hand, the algorithms of the cylinder construction method are different for each invariant set: they depend on whether the invariant set is an attractor or a repellor and on how many pieces it consists of. This requires a detailed topological analysis of each invariant set for any individual map to be investigated.

The other disadvantage of the cylinder set construction is that in order to obtain the level-n cylinder sets one has to store the end points of all cylinders on the previous level. The storage capacity requirement thus grows exponentially with increasing n. This gives a practical upper limit which is on the order of 20 for the level of cylinders which is often insufficient to obtain satisfactory asymptotics in n. On the other hand, we managed to combine the Frobenius-Perron method with an effective algorithm to track down a (in our case binary) tree of preimages whithout storing too much data. By this option it is possible to go as far as $n = 60$, even on a fast microcomputer.

Test programs proved that the difference between the results obtained by the two methods were in agreement far within the range of systematic errors. Our final numerical results were obtained, because of its advantages, by the constrained FPO method.

The determination of the asymptotic growth rates $\lim_{n\to\infty} |\psi_n(y)/\psi_0(y)|^{1/n}$ and then the free energy via (16) is based on the following considerations. The function sequence (20) at a given β value is expected to grow like

$$\psi_n(y) \approx A\lambda_1(\beta)^n + B\lambda_2(\beta)^n \tag{21}$$

provided that $\lambda_1(\beta)$ and $\lambda_2(\beta)$, the two dominant eigenvalues of $\hat{H}_\beta^{[X]}$, are discrete and n is big enough. In the numerical experiments, however, seldom does such a simple decay occur. Rather, these sequences are typically spoiled by strong oscillations. Because n is very much limited due to practical reasons, they cause uncertainty and a significant error in the final result.

The reason for these oscillations is that the eigensubspaces corresponding to the eigenfunctions of the constrained FPO are often degenerate. The simplest example we can give is the case of the three-piece attractor (or repellor): Due to the fixed visiting order among the three bands B_1, B_2, and B_3 [cf. Figs. 1(a)–1(c)], every eigenfunction of $\hat{H}_\beta^{[B]}$ is at least three times degenerate since one or two time steps transform the eigenfunctions into a linearly independent eigenfunction with the same eigenvalue. (It may happen that the degree of degeneracy is 6, 9, 12..., an integer multiple of 3.)

Owing to these degeneracies the time development of the ψ_n functions is described by

$$\psi_n(y) \approx A_{n \bmod d_1}\lambda_1(\beta)^n + B_{n \bmod d_2}\lambda_2(\beta)^n \tag{22}$$

rather than by (22). Here d_1 and d_2 stand for the de-

grees of degeneracy of the eigensubspaces belonging to the first and second eigenvalues $\lambda_1(\beta)$ and $\lambda_2(\beta)$, respectively. Our numerical method determines the values and the degrees of degeneracy of the two largest eigenvalues [29].

Another technical problem arises if the two eigenvalues $\lambda_1(\beta)$ and $\lambda_2(\beta)$ become close to each other. Then the rate of approaching the asymptotic exponent becomes infinitesimally small. Due to the limited number of available n's, this phenomenon, the critical slowing down of relaxation rates, is accompanied with extremely large errors of the estimated eigenvalues. This effect can be used to detect phase transitions in the dynamical system.

The numerical results presented below were obtained by the constrained FPO method with the filter set choices $X = B$, G, and A at different control parameter values.

B. Precritical situation

Figure 3(a) shows the results of numerical calculations obtained for the free energy functions of the precritical invariant sets. Apparently the $\beta F^{[G]}(\beta)$ function of the two-piece repellor is steeper than $\beta F^{[B]}(\beta)$ of the three-piece attractor, and, therefore, the relation $\lambda^{[G]} > \lambda^{[B]}$ holds for the respective Lyapunov exponents. The intersections with the vertical axis show that the topological entropy, $K_0^{[G]}$, is also greater than $K_0^{[B]}$, in accordance with our findings in Secs. III B b and III B c. This means that, in some sense, the repellor produces significantly stronger chaoticity in the system than the coexisting attractor, although its support is smaller in dimension.

The $\beta F^{[B]}(\beta)$ function incorporates the dynamical scaling exponents of the permanent chaos, while the $\beta F^{[G]}(\beta)$ function characterizes the dynamical properties of the transient chaotic motion. Although these functions cross each other at some β value below $D_0^{[G]} < 1$, their intersection cannot be interpreted as a phase transition since they represent different dynamics.

We would like to mention here that if the filter set X were chosen so as to contain both B and G, then — for certain initial functions ψ_0 and y values (cf. Sec. IV)

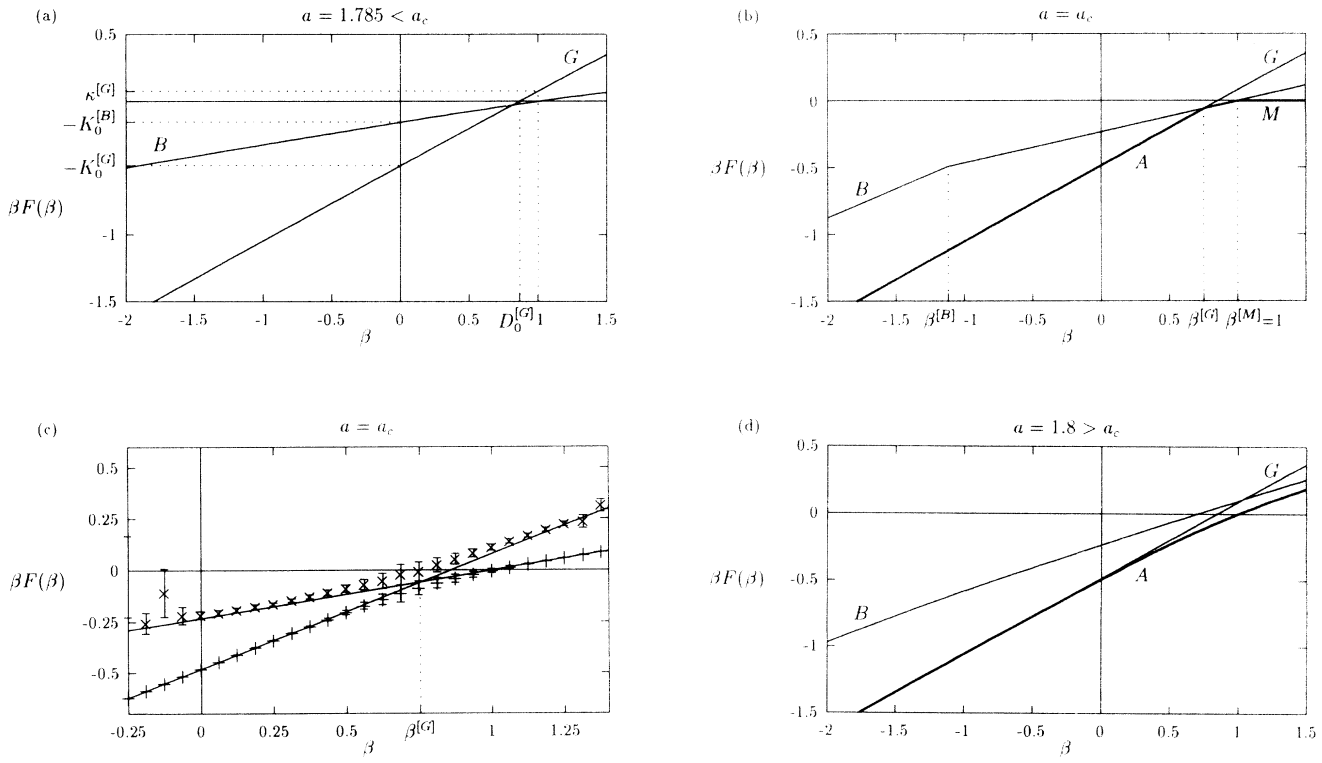

FIG. 3. The free energies of invariant sets obtained by the constrained FPO method. In the precritical regime (a) the independent free energies $F^{[B]}$ of the three-piece attractor in the band region and $F^{[G]}$ of the repellor in the gaps is shown. At the crisis (b) the attractor collides to the mediating orbit and this causes a break at $\beta^{[B]} \approx -1.119$ in $F^{[B]}$. The slope left of this breakpoint is Λ, the Lyapunov exponent of the mediating orbit which — being simultaneously the least unstable orbit of the repellor — also gives the asymptotic slope of $\beta F^{[G]}(\beta)$ for $\beta \to +\infty$. The newborn marginally stable heteroclinic orbit M contributes with $\beta F^{[M]}(\beta) \equiv 0$. The free energy of the full chaotic set A is the minimum of the three partial free energies (heavy line). Therefore it has two breakpoints at $\beta^{[G]} \approx 0.758$ and $\beta^{[M]} = 1$. The level crossing at crisis of the leading eigenvalues of the generalized FPO acting on the *entire* chaotic set A is also shown (c). The negative logarithms of the first (+) and second (×) eigenvalues approach the minimum and the maximum, respectively, of the partial contributions B and G (full lines). In the postcritical regime (d) the free energy of the entire attractor (A) runs somewhat below the contributions $F^{[B]}$ and $F^{[G]}$ of the repellor components. All free energy components, except $F^{[M]}$, were obtained after 30 – 60 iterations of the constrained FPO. The parameters are the same as in Fig. 1.

— the numerical results would yield the minimum of the two functions. In other words, at different β values the stronger chaotic exponents of the transient chaos would supress the exponents of the permanent chaos, or vice versa. The appearance of a virtual phase transition in this case would be an artifact only. Similarly, if X were extended so as to contain the isolated external fixed point x_*, then the free energy of this coexisting regular repellor, $\beta F(\beta) = \log|f'(x_*)|$, would imply the appearance of an additional false phase transition in the system [30] as it was pointed out by Refs. [31,26].

C. Crisis situation

Figure 3(b) shows the $\beta F(\beta)$ functions found numerically at the crisis situation $a = a_c$. The shape of the free energy of the two-piece repellor does not change much while the control parameter is going through a_c (cf. Sec. III B c).

The free energy function of the three-piece attractor, on the other hand, undergoes drastic changes at a_c. Numerically, the right side seems to be a straight line intersecting the horizontal axis at $\beta = D_0^{[B]} = 1$ as before, and the vertical axis at $-\log(2)/3$ since the topological entropy $K_0^{[B]}$ has reached its maximal value. The left side is another straight line having the slope of $\Lambda = \log\left[f^{(3)\prime}(x_a)\right]/3$, the local Lyapunov exponent of the period-3 orbit on the boundary. This is due to the fact that the attractor became fully developed after having been collided to the border of its domain, and, thus, a dynamic link has been created with the period-3 orbit $\{x_a, x_b, x_c\}$. The break at $\beta^{[B]} \approx (1 - \Lambda/K_0^{[B]})^{-1} = -1.119\,41$, where the two parts join each other, reflects a phase transition appearing because of this dynamical link. (This sort of phase transition is analogous to the case of a fully developed attractor at the external crisis situation, $a = 2$ [27].)

In order to gain the best understanding of the global changes of the thermodynamical behavior at crisis it is worth considering separately what happens if a_c is approached from below and from above.

In the limit $a \to a_c - 0$, there is still no dynamical link from B to G, therefore the corresponding free energies $F^{[B]}$ and $F^{[G]}$ describe independent dynamics, just like in the precritical region.

On the other hand, slightly above a_c the coupling between the two invariant sets is manifested in the appearance of orbits that are not restricted to either of the regions B or G. In the limit $a \to a_c + 0$, this dynamical coupling is infinitesimally weak, as if there were only a single, infinitely long trajectory mediating between B and G. Since the birth of this orbit happens just at $a = a_c$, it is marginally stable, and its free energy function is identically zero: $\beta F^{[M]}(\beta) \equiv 0$. This nicely reflects that attractor enlargement occurs together with an intermittent dynamics, often called crisis induced intermittency [7]. (It is well known that a vanishing free energy for $\beta \geq 1$ is always a sign of intermittent behavior [32].) The role of the marginal orbit in our case is analogous to that of a marginal fixed point in intermittent fully developed maps. Since there are three dynamical components with only infinitesimally weak couplings among them, the resultant free energy for $a \to a_c + 0$ is the absolute minimum of the free energies of the three components [the solid line in Fig. 3(b)], just like in the case of classical thermodynamics of coexisting phases.

The resultant free energy has thus two phase transition points, $\beta^{[G]} = 0.757\,99$ and $\beta^{[M]} = 1$, where the free energy function of the three-piece component intersects those of the two-piece and the mediating components, respectively. It is interesting that the fully developed three-piece invariant set (the old attractor) hardly contributes to the total free energy: apart from the small segment between $\beta^{[G]}$ and $\beta^{[M]}$, it is determined by the contributions of the former repellor in the gap region and the mediating orbit only. (The third transition at $\beta^{[B]}$, coming from the three-piece component alone, does not appear at all in the resultant free energy.)

Figure 3(c) shows the enlargement of the crossing of the three-piece chaotic attractor's and the two-piece repellor's free energy function around $\beta^{[G]}$ right at crisis. We have also depicted the values obtained by choosing $X = A = B \cup G$ for the two leading eigenvalues of the corresponding operator $\hat{H}_\beta^{[A]}$. The results clearly show that the first eigenvalue follows the maximum of the two subsystems' eigenvalue, while the second eigenvalue coincides with the minimum of them. The error bars themselves show that the error of the estimation due to the phenomenon of critical slowing down is indeed increased by magnitudes around the phase transition point, and has a maximum right there.

D. Postcritical situation

Figure 3(d) shows the thermodynamical potentials somewhat beyond the crisis situation. The two-piece and the three-piece invariant sets (both repellors now) form two subsets of the total invariant set of the attractor with free energy functions $\beta F^{[G]}(\beta)$ and $\beta F^{[B]}(\beta)$. Increasing the control parameter makes their fractal dimensions decrease and their escape rate increase continuously, while their topological entropies remain fixed. Although they no longer bear separate dynamical meaning in the asymptotic sense, they are still useful by serving as upper limits for the resultant free energy function of the whole invariant set, $F^{[A]}(\beta)$, or for characterizing finite time measurements. Since the escape from the former attractor is very infrequent and the corresponding dynamical link between B and G is very weak, we anticipate that $F^{[A]}(\beta)$ can be very well approximated by the minimum of the free energy functions of the two repellors.

Indeed, the $\beta F^{[A]}(\beta)$ curve of the enlarged attractor apparently runs below the curves belonging to the two repellor components. The breaks at the former phase transition points are smoothed out. These findings are the consequences of the nonzero contribution of the third component, the mediating orbits, to the total free energy.

Knowing the partial free energies $F^{[G]}(\beta)$ and $F^{[B]}(\beta)$,

however, is also useful since they contain information on the dynamical behavior *inside* the enlarged attractor A. In particular, close to a_c the escape rate, $\kappa^{[B]} = F^{[B]}(1)$, from the three-piece invariant subset gives $1/\tau$, the reciprocal of the average lifetime before bursts into the old (two-piece) repellor region G. The escape rate of the inverse process, $\kappa^{[G]} = F^{[G]}(1) \gg \kappa^{[B]}$, results in much shorter staying times in region G than in B.

VI. DISCUSSION AND CONCLUSIONS

By applying the concept of conventional thermodynamics [18,19], the Legendre transform of the free energy $F^{[X]}(\beta)$ yields an entropy, $S^{[X]}(E)$. This quantity characterizes the *dynamical* multifractal properties of the invariant set within X by specifying the topological entropy $S^{[X]}$ of its orbits with local Lyapunov exponent E as a convex function of E. In particular, the maximum of this function yields $K_0^{[X]}$, the topological entropy of the whole invariant set within X.

Figure 4(a) shows $S^{[G]}(E)$ and $S^{[B]}(E)$, the Legendre transforms of the free energies of the precritical two-piece repellor and three-piece attractor [cf. Fig. 3(a)]. It demonstrates spectacularly that in this case the transient chaos is indeed stronger than the coexisting permanent one: all local Lyapunov exponents occurring on the attractor are smaller than the minimal Lyapunov exponent on the repellor (which by chance happens to be Λ, the local Lyapunov exponent of the period-3 boundary orbit). Due to the properties of the Legendre transformation, the entropy curve of the attractor just touches the $S = E$ diagonal, while the repellor's spectrum is shifted by $\Delta E = \kappa^{[G]}$ to the right.

When the control parameter is increased to a_c, the boundary orbit belongs to both invariant sets (cf. Sec. II B). Figure 4(b) shows that in this case the period-3 orbit is the least unstable orbit on the repellor and the most unstable one on the attractor at the same time: the two entropy curves just touch each other at the common point $E = \Lambda$. The third partial entropy component, belonging to the marginally stable periodic orbit at birth, consists of a single point in the origin (M), and corresponds to the horizontal branch of the $\beta F^{[A]}(\beta)$ for $\beta > 1$. The entropy function of the invariant set of the whole A interval is obtained from the three partial entropy components as their convex hull. Thus the straight line segments with slopes $\beta^{[M]} = 1$ and $\beta^{[G]}$ are the Legendre transforms of the two phase transition points connecting the three-piece attractor's partial entropy function to the graphs belonging to the marginally stable orbit and the two-piece repellor, respectively.

In the postcritical regime the two chaotic sets within G and B remain joined at the period-3 orbit and, accordingly, the corresponding curves $S^{[G]}(E)$ and $S^{[B]}(E)$ still touch each other at $E = \Lambda$ [see Fig. 4(c)]. These functions describe the chaotic dynamics during the two intermittent chaotic phases which can be observed if the control parameter is not too far above the critical value a_c. Note that the $S^{[B]}(E)$ curve does not reach the diagonal any longer since the three-piece invariant set has turned to be a repellor. The entropy $S^{[A]}(E)$, characterizing the whole attractor, runs somewhat above the common envelope of the two components and extends to the diagonal. This "extra entropy" can be interpreted as the contribution of the orbits taking part in the coupling between the components. The most sensitive part of $S^{[A]}(E)$ is the one around the smallest accessible value of E. Since there are several very tiny periodic windows above crisis, it depends very strongly on the actual control parameter a. If one accidentally finds a marginally stable orbit at birth, the $S(E)$ function will be similar to that at the critical case with a zero minimal local Lyapunov exponent. At slightly different parameter values, however, the attractor may be strictly chaotic, yielding a positive lower bound for E. Then, the left part of the asymptotic result deviates from that obtained at crisis. For intermediate and large values of the exponent E one finds that the shape of the resultant entropy function is always close to the convex hull of the contribution of the basic components.

The concept we have outlined in this paper for determining dynamical properties via the thermodynamic potential of component chaotic sets can be easily applied to other one-dimensional maps. Moreover, by making appropriate generalizations in the definition of the thermodynamical quantities (cf. Ref. [33]) our method can be extended to multidimensional maps as well. Qualitatively the same phenomena should occur around internal crises of all dynamical mappings as we have demonstrated here on the example of the quadratic map (1).

If the system has certain symmetries, internal crises often happen as symmetry recovering attractor mergings [1]. Then the precritical attractors have identical free energy functions and the mediating orbit sits on the (chaotic or regular) saddle on the basin boundary between them. This latter invariant set plays the role of the repellor of our example.

Finally we would like to mention that the fact that the $S(E)$ functions of the disjoint components do not lap over is a consequence of the specific map, and this is not necessarily true for every one-dimensional map and is certainly atypical for higher-dimensional cases.

Our results support the view that the concept of multitransient chaos [17] can be applied usefully when weakly coupled repellors can be distinguished whithin a chaotic attractor: the weaker the coupling is, the better the scaling exponents, calculated from the individual components, approach that of the full attractor.

The importance of nonattracting chaotic sets very close to crisis has briefly been mentioned in a few previous publications [9,3] from the point of view of different multifractal spectra. Very recently, independently of our work, Leven *et al.* [13] have made several calculations for the $f(\alpha)$ spectrum and other metric quantities in the periodic window of a flow. Their results concerning the metric quantities associated with coexisting disjoint chaotic attractor and saddle are in accordance with our results in the precritical regime. We anticipate that in the postcritical regime the partial metric quantities, if someone measured them, would also behave analogously to our findings.

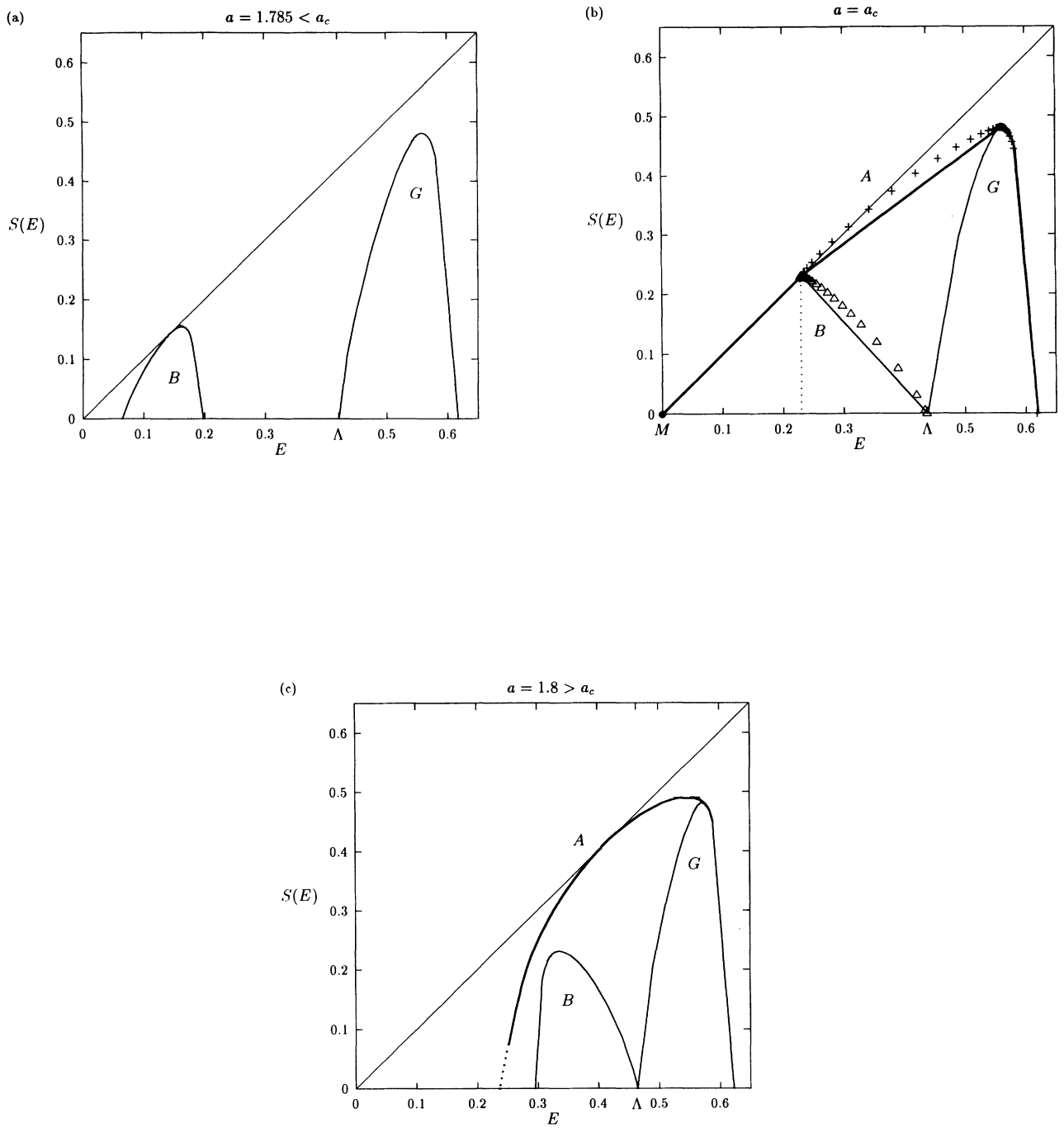

FIG. 4. Entropy spectra corresponding to the free energies of Fig. 3. In the precritical region (a) the entropy spectra of the three-piece attractor (B) and the coexisting repellor (G) describe independent dynamics ($a = 1.785$). At the crisis value (b), besides these, the contribution of the marginally stable heteroclinic orbit is a single point (M) in the origin. On arbitrary large but finite time scales G and B correctly reflect the dynamics. The asymptotically exact entropy of the entire system (A) is given by the convex hull (solid line) of the three components. The Legendre transforms of $F^{[A]}$ (+) and $F^{[B]}$ ($\triangle$) obtained numerically gradually approach the hull from above according to the rules of critical slowing down. In the postcritical region (c) the entropy spectrum B is shifted to the right, below the diagonal. The other basic component, G, remains practically unchanged. These spectra reflect short lifetime behaviors of the two intermittent chaotic phases. The entropy of the entire attractor (A) describing the asymptotic dynamics is somewhat over the convex hull of the two repellors. Note that despite the small change in the system parameter, the shape and the contribution of the three-piece invariant set undergo a drastic change in the course of attractor explosion.

ACKNOWLEDGMENTS

The authors acknowledge illuminating discussions with C. Beck, C. Grebogi, Lj. Kocarev, and Z. Kovács. This work has been supported by the Hungarian National Science Foundation (OTKA) under Grant Nos. 2090, T4439, and F4286. This research has partially been carried out with the financial help of the PHARE ACCORD Program, OMFB Grant No. H9112-0378.

[1] C. Grebogi, E. Ott, and J. A. Yorke, Phys. Rev. Lett. **48**, 1507 (1982); Physica D **7**, 181 (1983).

[2] T. L. Carroll, L. M. Pecora, and F. J. Rachford, Phys. Rev. Lett. **59**, 2891 (1987); W. L. Ditto *et al.*, *ibid.* **63**, 923 (1989).

[3] R. Stoop and J. Parisi, Phys. Rev. A **43**, 1802 (1991).

[4] J. C. Sommerer, W. L. Ditto, C. Grebogi, E. Ott, and M. L. Spano, Phys. Lett. A **153**, 105 (1991); J. C. Sommerer, in *Proceedings of the 1st Experimental Chaos Conference*, edited by S. Vohra *et al.* (World Scientific, Singapore, 1992), pp. 269–282; Phys. Lett. A **176**, 85 (1993); M. Franaszek and L. Fronzoni (unpublished).

[5] C. Grebogi, E. Ott, and J. A. Yorke, Phys. Rev. Lett. **57**, 1284 (1986).

[6] H. Ishii, H. Fujisaka, and M. Inoue, Phys. Lett. A **116**, 257 (1986); H. Uchimura, H. Fujisaka, and M. Inoue, Prog. Theor. Phys. **77**, 1344 (1987).

[7] C. Grebogi, E. Ott, F. Romeiras, and J. A. Yorke, Phys. Rev. A **36**, 5365 (1987).

[8] B. Pompe and R. W. Leven, Phys. Scr. **38**, 651 (1988).

[9] T. Horita *et al.*, Prog. Theor. Phys. **80**, 793 (1988); K. Tomita *et al.*, *ibid.* **80**, 953 (1988); K. Tomita *et al.*, *ibid.* **81**, 1124 (1989); S. Miyazaki *et. al*, ibid **82**, 863 (1989).

[10] J. C. Sommerer, E. Ott, and C. Grebogi, Phys. Rev. A **43**, 1754 (1991).

[11] H. Shibata, H. Fujisaka, and H. Mori, Phys. Lett. A **189**, 554 (1992).

[12] M. Franaszek and A. Nabaglo, Phys. Lett. A **178**, 85 (1993); **182**, 99 (1993).

[13] R. W. Leven, M. Selent, and D. Uhrlandt, Chaos Solitons Fractals (to be published).

[14] A. Hamm, T. Tél, and R. Graham, Phys. Lett. A **185**, 313 (1994).

[15] Y-C. Lai, C. Grebogi, and J. A. Yorke, in *Applied Chaos*, edited by J. H. Kim and J. Stringer (John Wiley, New York, 1992), pp. 441–456.

[16] T. Tél, in *Directions in Chaos*, edited by Hao Bai-lin (World Scientific, Singapore, 1990), Vol. 3, pp. 149–211.

[17] M. Franaszek, Phys. Rev. A **46**, 6340 (1992).

[18] J-P. Eckmann and D. Ruelle, Rev. Mod. Phys. **57**, 617 (1985); C. Beck and F. Schlögl, *Thermodynamics of Chaotic Systems — An Introduction* (Cambridge University Press, Cambridge, England, 1993).

[19] T. Bohr and D. Rand, Physica D **25**, 387 (1987); T. Bohr and T. Tél, in *Directions in Chaos*, edited by Hao Bai-lin (World Scientific, Singapore, 1988), Vol. 1, pp. 195–237.

[20] T. Tél, Phys. Rev. A **36**, 2507 (1987).

[21] P. Szépfalusy and U. Behn, Z. Phys. B **65**, 337 (1987).

[22] H. Fujisaka and M. Inoue, Prog. Theor. Phys. **78**, 268 (1987).

[23] A. Csordás and P. Szépfalusy, Phys. Rev. A **38**, 2582 (1988).

[24] M. J. Feigenbaum, J. Stat. Phys. **52**, 527 (1988).

[25] I. Procaccia and R. Zeitak, Phys. Rev. Lett. **50**, 2511 (1988); S. Vaienti, J. Phys. A **21**, 2023 (1988); **21**, 2313 (1988); J. Bene, Phys. Rev. A **39**, 2090 (1989); Z. Kovács, J. Phys. A **22**, 5161 (1989); H. Mori *et al.*, Prog. Theor. Phys. **81**, 60 (1989); T. Kobayashi *et al.*, *ibid.* **82**, 1 (1989); H. Fujisaka and H. Shibata, *ibid.* **85**, 187 (1991).

[26] Lj. Kocarev and Z. Tasev (unpublished).

[27] M. J. Feigenbaum, I. Procaccia, and T. Tél, Phys. Rev. A **39**, 5359 (1989).

[28] P. Szépfalusy, T. Tél, and G. Vattay, Phys. Rev. A **43**, 681 (1991).

[29] K. G. Szabó (unpublished).

[30] P. Cieslinski and M. Napiorkowski, Phys. Rev. A **41**, 2203 (1990).

[31] Z. Kovács (unpublished).

[32] P. Szépfalusy, T. Tél, A. Csordás, and Z. Kovács, Phys. Rev. A **36**, 3525 (1987).

[33] P. Cvitanović and G. Vattay, Phys. Rev. Lett. **71**, 4138 (1993).